Identification and probabilistic modeling of mesocrack initiations in 304L stainless steel

Jérémie Rupil, Ludovic Vincent, Stéphane Roux, François Hild

Identification and probabilistic modeling of mesocrack initiations in 304L stainless steel

J. Rupil,[a,b] L. Vincent,[a] F. Hild,[b] and S. Roux,[b*]

[a]CEA Saclay, DEN-DANS/DMN/SRMA/LC2M

F-91191 Gif sur Yvette cedex, France.

[b]LMT Cachan, ENS Cachan/CNRS/UPMC/PRES UniverSud Paris

61 avenue du Président Wilson, F-94235 Cachan cedex, France.

September 19, 2010

Abstract

A probabilistic model is proposed to simulate the growth of fatigue damage in an austenitic stainless steel at a mesoscopic scale. Several fatigue mechanical tests were performed to detect and quantify mesocrack initiations for different loadings by using digital image correlation. The number of initiated mesocracks is experimentally determined. The process is then described by a Poisson point process. The intensity of the process is evaluated by using a multi-scale approach based on a probabilistic crack initiation law in a typical grain.

*Corresponding author. Email: stephane.roux@lmt.ens-cachan.fr

Keywords: Crack initiation; Digital image correlation; Identification; Mechanical fatigue; Poisson point process.

1 Introduction

Many industrial structures are submitted to mechanical or thermal fatigue loadings. If the material has no initial bulk or surface defects, a fatigue loading level greater than the fatigue limit initiates a critical damage (Ewing and Humfrey, 1903). For the two types of loading, namely mechanical or thermal, the major part of damage growth before fracture consists of random multi-initiations of short cracks on the surface. This phenomenon finally leads to the growth of either a main macrocrack in mechanical fatigue, or a crack network in thermal fatigue. In this paper we focus on the quantification of the multi-initiation stage of short cracks, which is a common feature of thermal and mechanical fatigue (Maillot, 2003).

It has been established in monocrystalline materials (Mughrabi et al., 1979) that microcrack initiation is based on dislocation pile up in Persistant Slip Bands (PSB) on the surface grains. These PSBs induce a surface topography, which is experimentally observed and quantified (Mughrabi et al., 1983; Ma and Laird, 1989; Man et al., 2002), called extrusions and localized in bands. The induced local stress concentrations on these bands may eventually induce the nucleation of a transgranular microcrack. The physical mechanism of crack initiation is now well described in the literature for monocrystalline material and will not be discussed herein. Moreover, the phenomenon of local initiation in one grain has already been modeled the-

oretically (Mura, 1994), and numerically by discrete dislocations dynamics simulations (Déprés et al., 2006).

After nucleation, the microcrack mainly follows a shear stress propagation mode along PSBs. This phase corresponds to stage I of fatigue crack growth (Forsyth, 1961). The study presented herein focuses on the next stage corresponding to the transition from the shear stress propagation mode in one grain to the normal stress propagation mode across several grains. In this phase, the propagation is microstructure-dependent. The crack may often be pinned at grain or twin boundaries. The latters represent barriers for classical propagation modes based on Stress Intensity Factors (SIF) computations. In that case and when the initiated microcrack density is large enough, crack growth by coalescence of neighboring microcracks is effective (Magnin et al., 1985).

Some authors (Lindborg, 1969; Fedelich, 1998; Zhai et al., 2000) then proposed different solutions to model the coalescence of microcracks. Another numerical study (Hoshide and Socie, 1988) simulated the competition between the two types of propagation modes. When the crack becomes large enough, the propagation can only be described by a self-propagation mode based on SIFs. The assumption is made that if the short crack is long enough (compared with the characteristic size of the microstructure) to have a growth well described by a deterministic propagation law then it is called mesocrack. At this stage, the mesocrack is still not in Paris' (Paris and Erdogan, 1963) propagation regime but is no more microstructure-dependent (*i.e.,* it is physically short but microstructurally long (Miller, 1997)).

The behavior of a unique mesocrack from its microstructural size to a

(potentially fatal) macrocrack is modeled with the use of a propagation law representative of short cracks. A recent probabilistic model (Malésys et al., 2009) proposes to simulate the behavior of multiple mesocracks in an interacting network. This model needs data on mesocrack initiation. Hence, the main objective of this paper is to propose a probabilistic law for the change of the mesocrack density in uniaxial mechanical fatigue. This law describes the local (random) conditions for microcrack initiations as discussed before.

Several stochastic models have been proposed to simulate mesocrack densities. They are often based on Monte-Carlo simulations (Suh et al., 1992; Bataille and Magnin, 1994; Argence, 1996; Osterstock et al., 2007) and identified by using few experimental data. Since the initiation phenomenon in fatigue occurs generally on the surface and at a very small scale, classical macroscopic measurements do not allow the experimentalist to get quantitative data of this process. For example, damage quantification based on Young's modulus variations (Desmorat et al., 2007) can only describe the initiation of a macrocrack (corresponding to 90 % of fatigue lifetime). The process modeled herein starts from 10 % of fatigue lifetime and mesocrack initiation occurs around 60 % of fatigue lifetime (Magnin et al., 1985).

The only way to identify a model is therefore to perform fatigue mechanical tests with microcrack detection methods. Several techniques are currently used, namely, replica (Chauvot and Sester, 2000), in situ optical (Malésys, 2007; El Bartali et al., 2008) or SEM (Vasek and Polak, 1991) observations. Application of such techniques is most of the time long and difficult. However, multi-initiations of short cracks at the mesoscopic scale have been observed for uniaxial (Hua and Socie, 1984; Magnin et al., 1985)

and more complex loadings (Weiss and Pineau, 1993). As existing experimental data are scarce, new tests were performed for the studied material. The experimental quantification of the phenomenon is difficult because of the size of the cracks compared with that of the gauge surface. Moreover neither the location nor the number of cycles to initiation are well known. Therefore, in many studies the surface of crack detection is very small to locate more easily the cracks. However, it is more difficult to have a statistically representative surface. Several tests were performed with the use of a Digital Image Correlation (DIC) technique at the mesoscopic scale using a digital camera. This approach is not as accurate as the techniques alluded to before, but it allows us to couple two experimental constrains, namely, fine local heterogeneity quantifications and fast visualization of damage growth.

The paper is divided into three parts. In the first one, the experimental procedure and the results are presented. The modeling strategy used to derive the mesocrack initiation density is discussed in the second part. Last, the experimental results are compared with the predictions given by the probabilistic model.

2 Experimental procedure

2.1 Experimental setup

The studied material is an AISI 304L stainless steel. It is one of the main materials used to make pipes in nuclear power plants. It is a polycrystalline austenitic steel (Figure 1) containing residual ferrite (approximatively

4 wt%). The average grain size is equal to 40 μm.

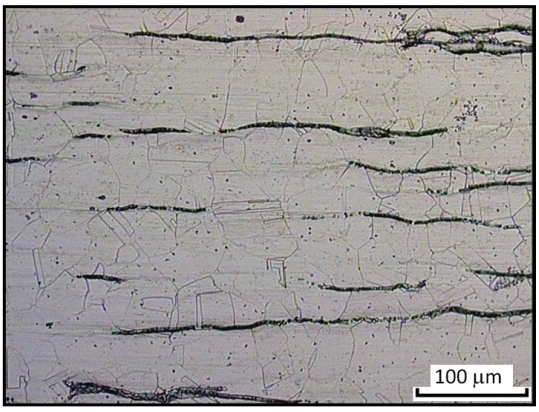

Figure 1: 304L microstructure made of austenitic grains (gray) with ferritic residual grains (black).

The global geometry of the specimen (Figure 2) is similar to classical fatigue samples. To monitor the damage stage with DIC, a gauge surface is obtained by machining a planar zone (Figure 2). This type of notched geometry has already been successfully used (Vasek and Polak, 1991; Malésys, 2007) for observations of crack initiations. The geometry was slightly modified to obtain a larger surface of observation. The shallow notch creates a local stress heterogeneity on the surface in order to localize initiations. The notch area is mechanically polished. A final electropolishing is performed resulting in a good quality of the surface finish suitable for optical observations. Figure 1 shows a microscopic observation carried out after surface polish. The stress and strain concentrations due to the notch were estimated to be equal to 1.05 (Polak and Zezulka, 2005).

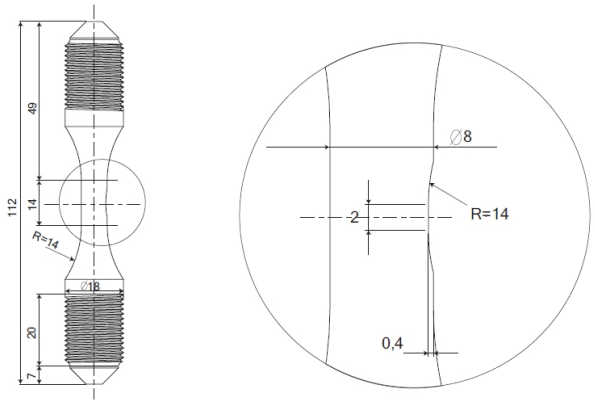

Figure 2: Geometry of the specimen with a flat part (0.4 mm in depth) in the center of the gauge zone (Malésys, 2007)

Specimens are cycled by sine-wave loading (5 Hz frequency) in a servohydraulic fatigue testing machine . Stress amplitude $\frac{\Delta\sigma_{xx}}{2}$ is controlled for all the tested samples. The total strain is measured by an extensometer (gauge length: 10 mm). Periodically (the period depends on the test, namely, around 10% of the fatigue life), the maximum load is maintained during $0.2s$ and a picture acquisition is automatically triggered. The images are captured with a digital single lens reflex camera (CANON EOS 5D) and a macro lens (CANON MPE65) with a magnification of $\times$ 5. The data are gray level raw images with a resolution of 3 Mpixels for a notch surface of 3×5 mm^2. The final pixel size on the raw pictures is 3.2 μm. Contrary to other methods used for visual crack detection (*e.g.,* based on SEM or optical microscope observations), the raw pictures (Figure 3a) cannot be used because the pixel size prevents any observation of small cracks with an opening less than 3.2 μm. The cracks are detected on the raw images only when their sizes reach half

the width of the notch. Therefore, the quantification of mesocrack densities is only possible with the use of a post-processing technique.

2.2 Full field measurement technique

In the present case DIC is used to detect and quantify mesocrack initiations. DIC is based on the minimization of the correlation residuals between the two considered images. Let f denote the reference picture, g that of a later state of the observed surface, and $\underline{u}(\underline{x})$ the unknown in-plane displacement at the (pixel) location $\underline{x}$. The local correlation residual

$$\varphi(\underline{x}) = |f(\underline{x}) - g(\underline{x} + \underline{u}(\underline{x}))| \tag{1}$$

consists in computing the gap to brightness conservation. Its dimensionless counter-part $\tilde{\varphi}$ is obtained by dividing φ by the dynamic range of the reference picture (*i.e.,* $\max(f) - \min(f)$). In the present case a global approach to DIC is chosen. Consequently, the global residual defined over the region of interest (ROI)

$$\Phi^2 = \int_{\mathrm{ROI}} \varphi^2(\underline{x}) \mathrm{d}\underline{x} \tag{2}$$

is minimized with respect to the kinematic unknowns. The latters are the degrees of freedom associated with a Q4 finite element discretization based on 4-noded elements (with bilinear interpolations). It is therefore referred to as Q4-DIC (Besnard et al., 2006). One classical way of obtaining a good texture is to spray paint to get a random pattern. However, the paint may hide microcrack initiations. As in other experimental studies (Malésys, 2007; El Bartali et al., 2008), the texture is the natural contrast of the revealed microstructure.

As in finite element computations, the ROI is uniformly meshed with Q4 elements each made of a square of $\ell \times \ell$ pixels, so that ℓ defines the element size. The technique gives access to the displacement field in each pixel of any element of the ROI. At the beginning of the test, there is no crack on the surface. The images are taken for the same load level. Consequently, the displacement field only corresponds to the residual strains due to cyclic hardening or softening (and a possible rigid body motion). A typical result is shown in Figure 3 for a test with $\frac{\Delta\sigma_{xx}}{2} = 200$MPa. The reference picture is shot at the maximum level of the first cycle. The second picture is then shot after 30,000 cycles. The measured displacement field in the loading direction

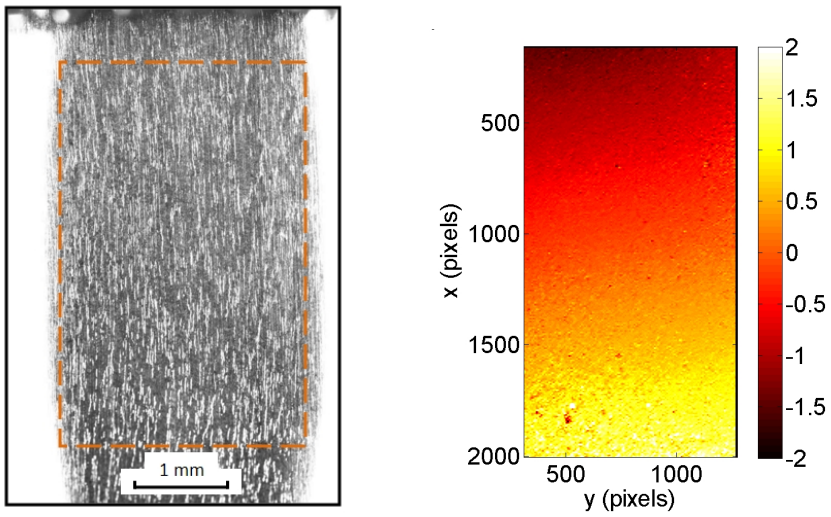

(a) (b)

Figure 3: (a) Raw picture and region of interest (dashed box). (b) Longitudinal displacement field (in pixels) after 30,000 cycles (1 pixel $\leftrightarrow$ 3.2 μm)

is shown in Figure 3b. This map shows a displacement gradient related

to cyclic softening of the material. For this material (304L) and for the studied domain of fatigue lifetime (*i.e.,* > 10,000 cycles), the cyclic behavior is composed of three phases, namely, primary hardening, cyclic softening and finally secondary hardening (Poncelet et al., 2010; Colin et al., 2010). Since the behavior is not stabilized in the presented test, the reference image is from now on chosen to be the first one just after cyclic softening. As a consequence, the mean strain between the two images used for correlation is minimized.

To assess the quality of the texture, the measurement uncertainty is evaluated a priori on the considered reference picture (Besnard et al., 2006). It is obtained by prescribing a known displacement (here 0.5 pixel, which is known to be the worst case because of gray level interpolation bias). The comparison between the measured displacement and the prescribed one gives the bias (which is negligible) and the standard deviation, providing an evaluation of the displacement uncertainty. The relationship between the standard uncertainty and the element size follows a power law

$$\sigma_u = \frac{A^{\alpha+1}}{\ell^{\alpha}} \tag{3}$$

where σ_u is the standard displacement uncertainty, and A, α are two constants. The identified values are $A = 1.15$ pixel, and $\alpha = 1.7$.

This first analysis only evaluates the intrinsic performance of the correlation code with the texture at hand (labeled "computational uncertainty" in Figure 4). However, it does not take in account the uncertainty resulting from experimental conditions. Therefore, the resolution has also been quantified. Just before the starting the test, 10 images are shot for a fixed load

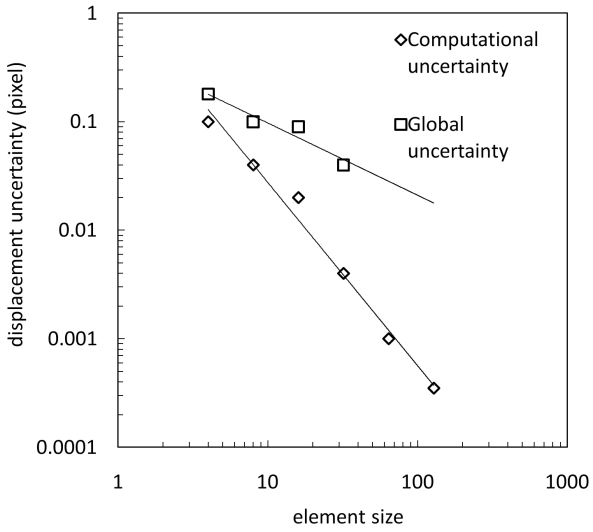

Figure 4: Uncertainty and resolution analyses. Standard displacement uncertainty as a function of the element size ℓ.

level close to zero. For each picture a displacement measurement is performed for different element sizes. For each couple of images and element size, the displacement field corresponds to a distribution of local displacements. From these distributions, the mean value and the standard deviation are computed. The latter is compared with the value observed in the uncertainty analysis. This (experimental) approach takes all the sources of uncertainty (labeled "global uncertainty" in Figure 4) into account such as testing machine vibrations, acquisition noise, lighting conditions. The graph shows that for small element sizes most of the uncertainty comes from the correlation code whereas for large elements, the correlation uncertainty is very low compared to that caused by the experimental conditions.

Let us now assume that a crack has appeared on the surface. In the

literature, DIC has already been used to detect crack propagation (Sutton et al., 2001; Hamam et al., 2007). In most cases large cracks are studied, with various opening levels. In the present case the displacement field is analyzed. In particular, in the vicinity of small cracks, the displacements become discontinuous. As a consequence, local displacements around the crack are slightly altered. Figure 5a shows the same type of result as Figure 3b but after 80,000 cycles of loading. This stage corresponds to the first detection of mesocrack initiation.

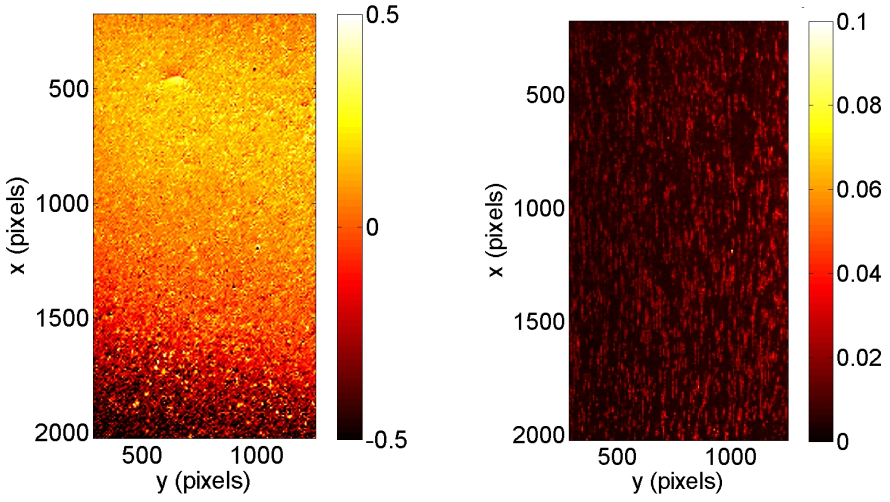

(a) (b)

Figure 5: (a) Longitudinal displacement field in pixel (1 pixel $\leftrightarrow$ 3.2 μm). (b) Normalized correlation residual field $\tilde{\varphi}$.

The use of 4-pixel elements gives the best (*i.e.*, lowest) spatial resolution in terms of crack detection. Let us emphasize that this low value is remarkable in view of the texture at hand. Such low sizes are accessible only thanks to the global approach to DIC used herein. The quantification of the uncertainty shows that for the smallest elements used (*i.e.*, $\ell = 4$ pix-

els) the standard displacement uncertainty is about 0.2 pixel (or 0.6 μm). The measured level of crack opening is at most of the order of 0.4 pixel (or 1.3 μm). The total range of the displacements shown in Figure 5a is equal to 1 pixel. All the displacements are less than 1 pixel (or 3.2 μm). This result leads to several conclusions. First, for crack openings less than the pixel size, the crack is not detectable on the residual map (Figure 5b). Second, the uncertainty evaluation gives also a good estimate of the threshold for crack detection using a DIC technique. Experimentally a crack is detectable when its opening is greater than 0.4 pixel, which is twice the standard displacement uncertainty. This type of crack has a length of about 150 μm (or 4 grains).

2.3 Experimental results

The DIC technique is performed for all the recorded pictures and multi-initiation is noted on the next displacement field maps. Figure 6a illustrates this result and corresponds to the displacement field after 120,000 cycles of loading. The test is interrupted when the macrocrack traverses the whole flat part (for the case presented, it corresponds to 132,000 cycles). At this stage the specimen is not broken yet and a change of macroscopic data (*i.e.,* strain given by the extensometer) only begins to be observed. Quantitatively, the two biggest mesocracks have an opening greater than the pixel size and they are now appearing on the correlation residual map (Figure 6b).

In the following, the main results concerning crack density changes are presented. The density is computed as the number of cracks "manually" counted on the pictures (as in Figure 6a) and divided by the area of the

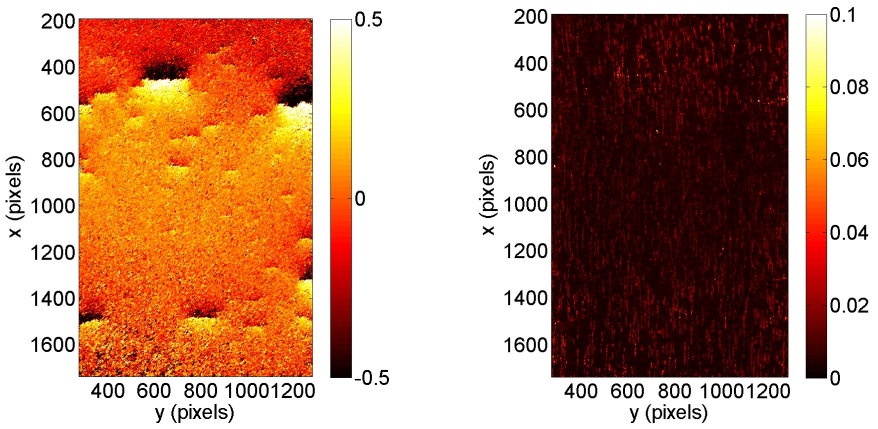

(a) (b)

Figure 6: (a) Longitudinal displacement field in pixel (1 pixel $\leftrightarrow$ 3.2 μm). (b) Normalized correlation residual field $\tilde{\varphi}$.

ROI. This choice is made even though the notch induces a (small) local stress heterogeneity. This hypothesis is experimentally confirmed since at the end of the test the major part of the notch is covered with cracks (Figure 6a). For a particular load level (*i.e.,* 210 MPa), several results are collected. The mesocrack density change is shown in Figure 7. The points represent the mesocrack density change for 5 specimens labeled A26-xxx. The number of cycles to fracture lies between 50,000 and 75,000 cycles. All the densities are given for a number of cycles (N) divided by the number of cycle when the test was interrupted (NR).

Figure 7 illustrates the uncertainty related to the density change with the 'same' material (taken from the same raw bar) and at the same loading level. The beginning of initiation is always around 60 and 70 % of lifetime but the final density varies between 1 and 3 cracks / mm^2. It confirms the randomness of the crack initiation process but shows also the same effect in terms of

mesocrack densities. It also proves the need for performing several tests for each load level to have a good estimate of the probabilistic parameters (*e.g.,* mean and standard deviation) associated with the initiation process.

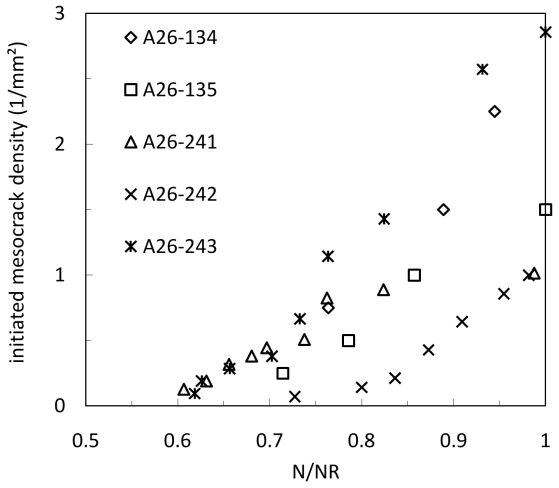

Figure 7: Density changes with the normalized number of cycles for 5 specimens with the same load level.

Figure 8 shows the comparison of 4 tests at different load levels ranging from 190 to 220 MPa. In the 220 MPa loading level case, the density at the end of the test is less than that obtained for lower loading levels such as 210 or 200 MPa. Post-mortem observations using optical microscopy for each test revealed that the 220 MPa test presents a larger density of small cracks (length less than $150\mu m$) than the other tests (with a lower loading level). This result confirms that for high stress levels, most of the short cracks are pinned on grain or twin boundaries, and do not find the right conditions in the neighboring grain to become long enough to be detected by the DIC technique. It also reveals the competition between multiple

mesocrack initiations and propagation of the first initiated mesocrack leading to failure. In the 220 MPa case, the first mesocrack propagation is too fast to let numerous other mesocracks initiate on the surface.

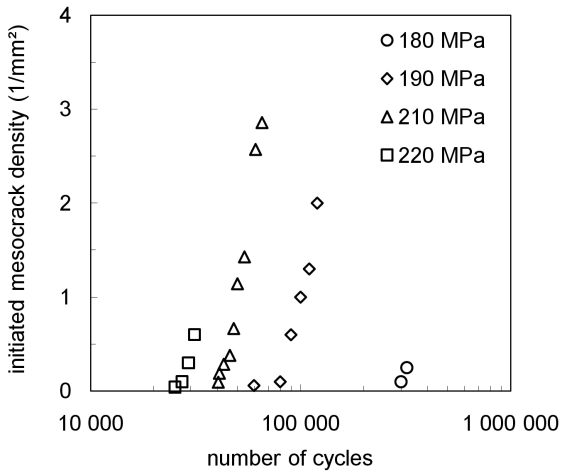

Figure 8: Density changes for 4 specimens with different stress levels.

3 Probabilistic modeling

The initiation of microcracks is modeled by a Poisson Point Process (PPP) (Denoual et al., 1997; Doudard et al., 2005; Malésys et al., 2009)

$$P(N_\mu = \nu, \Omega) = \frac{(\lambda Z)^\nu}{\nu!} \exp(-\lambda Z) \tag{4}$$

where $P(N_\mu = \nu, \Omega)$ denotes the probability of finding ν cracks in domain Ω, Z the surface of Ω where initiation takes place, and λ the intensity of the PPP (*i.e.,* the mean mesocrack density). This type of law has been experimentally confirmed for crack initiations (Weiss, 1992).

The intensity λ of the PPP has to be identified. Moreover, this variable depends mostly on the loading and the number of cycles N. Malésys *et al.* (2009) proposed an approach based on Weibull's theory (*i.e.,* λ is given by a power function of the stress amplitude). This theory only uses the endurance stress and the standard deviation to identify the parameters of that function. However, the extension of the theory to higher load levels turned out to be quite far from experimental results. The objective is to propose a new law for λ in the high and intermediate levels of loading. The intensity is modeled by a function Ψ to be determined

$$\lambda = \Psi(\Delta\sigma, N, ...) \tag{5}$$

where Ψ may depend on a macroscopic loading variable such as the stress amplitude $\Delta\sigma$, on the number of cycles N, and possibly on other parameters to be determined.

The starting point of the model developed herein is to quantify the probability of initiating a microcrack in a single grain. The main condition for microcrack initiation is given by the height of extrusion/intrusion profiles which is related to the level of local plastic strain amplitudes in the grain as a first approximation. At the scale of the aggregate, the mechanical fields are necessarily heterogeneous due to the complex interactions between grains of different shapes and crystallographic orientations. If this aggregate is loaded in fatigue with a macroscopic stress inducing a macroscopic plastic strain, each grain of the aggregate is going to experience a different local plastic strain level, and thus a different probability of initiating a microcrack after N cycles. To relate the plastic strain and the number of cycles to crack

initiation, Mura (1994) proposed a theoretical model for uniaxial loadings. Déprés (2004) also proposed an initiation law for uniaxial and biaxial loadings as well. These two types of model lead to the same conclusion concerning the uniaxial case without mean stress effects. The number of cycles to initiation N_i is written as

$$N_i = \frac{F(D_g, \gamma, K)}{{\Delta\epsilon_p}^2} \tag{6}$$

where F is a function depending on several parameters such as the characteristic grain size D_g, the criterion for surface creation γ and a constant K.

For each grain several parameters in this law are different, mainly the geometry and the mean plastic activity. Déprés' law (2004) is used and two variables become probabilistic, namely, the depth of the grain (h_g, representing the geometric randomness) and the local plastic strain ($\Delta\epsilon_p$, representing the local loading variations)

$$\sqrt{N_i} = \frac{D_g \gamma}{k h_g \Delta\epsilon_p} \tag{7}$$

where D_g is equal to 40 μm, and γ is equal to 0.75 (Osterstock, 2008). The last parameter k will be identified using the above presented experimental results. Maillot (Maillot, 2003) shows that the grain size distribution for this material is log-normal

$$p(h_g) = \frac{1}{h_g \sigma_h \sqrt{2\pi}} \exp\left[-\frac{1}{2}\left(\frac{\ln(h_g) - \mu_h}{\sigma_h}\right)^2\right] \tag{8}$$

with

$$\mu_h = \ln\left(\frac{E(h_g)^2}{\sqrt{E(h_g)^2 + Var(h_g)}}\right) \tag{9}$$

and

$$\sigma_h^2 = \ln\left(\frac{Var(h_g)}{E(h_g)^2} + 1\right) \tag{10}$$

The parameters $E(h_g)$ and $Var(h_g)$ denote respectively the expectation and variance of the distribution. The following values are chosen: $E(h_g) = D_g/2$ and $Var(h_g) = E(h_g)^2/16$. $p(h_g)$ is the probability density function (pdf) of the log-normal distribution. The plastic strain distribution is also assumed to be log-normal. The first comparisons with polycrystalline computations show that this hypothesis is reasonable (Le Pecheur, 2008; Sauzay et al., 2010; Li, 2011). The pdf is the same as in Equation (8). The polycrystalline computations cited before also motivate the choice of the mean and variance such that $E(\Delta\epsilon_p) = \Delta E_p$ and $Var(\Delta\epsilon_p) = \Delta E_p^2/9$, ΔE_p being the macroscopic plastic strain. One additional hypothesis is the statistical independence of the two variables. Equation (7) is also written as

$$\ln(\Delta\epsilon_p) + \ln(h_g) = \ln(K) - \frac{\ln(N_i)}{2} = \Delta \tag{11}$$

with

$$K = \frac{D_g\gamma}{k} \tag{12}$$

The variable Δ (as the sum of two Gaussian independent random variables, $\ln(\Delta\epsilon_p)$ and $\ln(h_g)$) also follows a normal distribution. The probability of initiating a crack before a given number of cycles N is equal to the cumulative probability of the normal distribution Δ

$$P(N_i < N) = \frac{1}{2}\left[1 - \mathrm{erf}\left(\frac{\ln(K) - (1/2)\ln(N_i) - \mu_\Delta}{2\sqrt{2}\sigma_\Delta}\right)\right] \tag{13}$$

with

$$\mu_\Delta = \mu_h + \mu_{\Delta\epsilon_p} \tag{14}$$

and

$$\sigma_\Delta = \sqrt{\sigma_\Delta^2 + \sigma_{\Delta\epsilon_p}^2} \tag{15}$$

It is possible to obtain (see Equation (13)) and compute the probability of having one microcrack in one grain of the aggregate for different applied loadings (Figure 9).

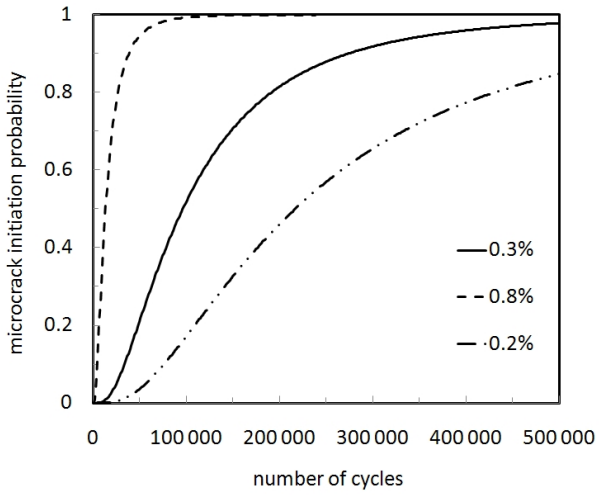

Figure 9: Probability of initiating a microcrack for different macroscopic plastic strain variations.

Let us now focus on the calculation of the mesocrack density. An aggregate made of n grains aligned along one direction (1D problem), and subjected to a uniaxial loading (perpendicular to the direction of the grain alignment). For each number of cycles, the probability of crack initiation is the same for all the grains and corresponds to $P(N_i < N) = P$. The microscopic growth of cracks is assumed to be described by coalescence (Lindborg, 1969). This assumption induces the coalescence of 2 neighboring microcracks

forming a longer microcrack. The same process enables for the creation of cracks of length 3, 4, 5, etc. grains. The condition of having an amount of k cracks aligned among the n grains is that each amount of k grains should be surrounded by 2 grains that did not initiate a crack. Let P denote the probability of initiation and $Q = 1 - P$ the probability of non initiation. The number of amounts of k initiated grains A_k reads

$$A_k = nQ^2P^k \tag{16}$$

The number of cracks we are interested in for comparison purposes with the experimental results is cracks of length equal to or greater than m grains. This number of cracks $A_{>m}$ is given by

$$A_{>m} = \sum_{i=m}^{n} nQ^2P^i = nQ^2P^m(1 + P + P^2 + ... + P^{n-m}) \approx nQP^m \tag{17}$$

and the density is obtained by dividing the number of cracks by the considered surface S. For the sake of simplicity, a square shape is assumed for the aggregate so that $S = nD_g^2$. Moreover, in the 2D case, the microstructure is described by a regular array of square grains. The density of cracks whose length is larger than m grains becomes

$$\lambda_m = \frac{1}{D_g^2}(1 - P(N_i < N))P(N_i < N)^m \tag{18}$$

There is one remaining parameter to be identified, namely, the initiation coefficient k of Equation (7). The experimental results for the particular loading of 210MPa shown in Figure 7 are used to identify $k = 1.75$.

4 Comparisons with experiments

Two comparisons are carried out. The first one concerns the above presented experimental results, and others found in the literature (Bataille and Magnin, 1994) in which the density change of smaller crack sizes were detected.

4.1 Comparisons for the different load levels

The density we are interested in for comparison purposes with the experimental results is for cracks whose length is greater than or equal to 4 grains (*i.e.*, the length that is detected with the correlation technique, see Section 2.2). The density is given by

$$\lambda = \frac{1}{D_g^2}(1 - P(N_i < N))P(N_i < N)^4 \tag{19}$$

The results for the mean density is compared with the experimental result of Figure 10. The model describes well the impact of plastic strain on the density change. When the load level becomes closer to the fatigue limit, the assumption of large microcrack densities becomes less valid. As a consequence, the model predicts a mesocrack density greater than the one recorded (see case 180 MPa in Figure 10). Hence, for low loading levels, a threshold on the plastic strain amplitude may be added in the initiation criterion. Such a modification in the model would delay the mesocrack initiations only for low loading amplitudes.

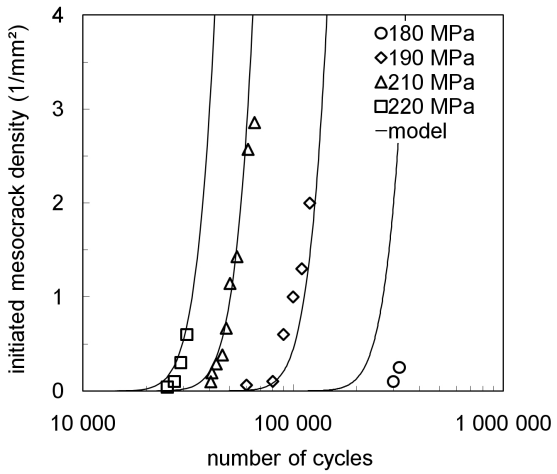

Figure 10: comparison between experimental crack densities evolution and model prediction

4.2 Comparison for different crack sizes

Magnin *et al.* (1985) performed a uniaxial mechanical fatigue test with a high level of plastic strain on a 316L stainless steel and recorded the crack density changes using a replication technique. This technique is long to set up but allows them to detect one grain-long microcrack (called type I). The results are reported in Figure 11a. They also noted the mesocrack density changes for type II cracks (between 2 and 3 grain long) and type III cracks (sizes greater than or equal to 4 grains). Figure 11b shows the predictions of the model developed herein. The value of the k parameter is identical to that determined for 304L stainless steel. Without any modification of the model or parameters, a good agreement is observed. This result shows that the predictive capacity of the present model is good.

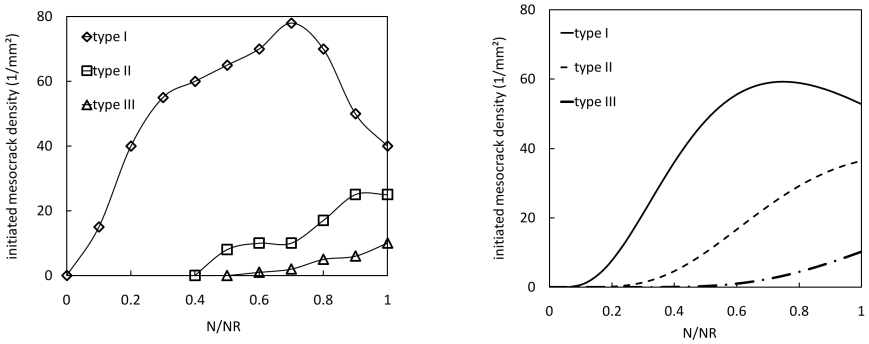

(a) (b)

Figure 11: (a) Experimental results for multiple initiation of microcracks (type I), short mesocracks (type II) and mesocracks (type III) after Bataille and Magnin (Bataille and Magnin, 1994). (b) Model predictions for the same type of crack density changes.

5 Summary

Several uniaxial fatigue mechanical tests in tension-compression have been performed on a 304L stainless steel. A flat part on the specimen gauge surface is monitored with a classical digital camera. The use of the raw pictures coupled with a global digital image correlation technique enables us to follow the crack density changes for mesocracks longer than $150\mu m$.

A probabilistic model for microcrack nucleation and coalescence is proposed and leads to a good agreement with the experimental results. While most of existing models are based on numerical Monte Carlo simulations, the model presented herein gives an analytical law only dependent on the microstructure size and the macroscopic plastic strain distributions. The particular case of low fatigue loading is not currently well simulated since no threshold parameter on the plastic strain is used.

The approach developed herein can be improved by using numerical results of discrete dynamic dislocation or polycrystalline finite element simulations. The remaining hypothesis concerning local heterogeneity for the plastic strain and the independence between the microstructure and the plastic strain will be studied by performing polycrystalline finite element simulations on "real" aggregates of 304L stainless steel. Moreover, this study reveals the need for more experimental data at the smallest scales. In that way, improvement in DIC technique for microcrack detection could lead to a better understanding of the local phenomenon driving initiation and propagation of microcracks.

References

Argence, D. (1996). *Endommagements couplés de fatigue et de fluage sous chargement multiaxial*. PhD thesis, Ecole des Mines de Paris.

Bataille, A. and Magnin, T. (1994). Surface damage accumulation in low-cycle fatigue - physical analysis and numerical modeling. *Acta Metallurgica Et Materialia*, 42:3817–3825.

Besnard, G., Hild, F., and Roux, S. (2006). Finite element diplacement fields analysis from digital images: Application to portevin-le chatelier bands. *Experimental Mechanics*, 46:789–803.

Chauvot, C. and Sester, M. (2000). Fatigue crack initiation and crystallographic crack growth in an austenitic stainless steel. *Computational Materials Science*, 19:87–96.

Colin, J., Fatemi, A., and Taheri, S. (2010). Fatigue behavior of stainless steel 304l including strain hardening, prestraining, and mean stress effects. *Journal of Engineering Materials and Technology*, 132:021008,1–13.

Denoual, C., Barbier, G., and Hild, F. (1997). A probabilistic approach for fragmentation of brittle materials under dynamic loading. *Comptes Rendus De L'Academie Des Sciences Série Ii Fascicule B-Mécanique Physique Astronomie*, 325:685–691.

Déprés, C. (2004). *Modélisation physique des stades précurseurs de l'endommagement en fatigue dans l'acier inoxydable austénitique 316L.* PhD thesis, Institut national polytechnique de Grenoble.

Déprés, C., Robertson, C., and Fivel, M. (2006). Low-strain fatigue in 316l steel surface grains: a three dimension discrete dislocation dynamics modelling of the early cycles. part 2: Persistent slip markings and micro-crack nucleation. *Philosophical Magazine*, 86:79–97.

Desmorat, R., Kane, A., Seyedi, M., and Sermage, J. (2007). Two scale damage model and related numerical issues for thermo-mechanical high cycle fatigue. *European Journal of Mechanics a-Solids*, 26:909–935.

Doudard, C., Calloch, S., Cugy, P., and Hild, F. (2005). A probabilistic two-scale model for high-cycle fatigue life predictions. *Fatigue and Fracture of Engineering Materials and Structures*, 28:279–288.

El Bartali, A., Aubin, V., and Degallaix, S. (2008). Fatigue damage analysis in a duplex stainless steel. *Fatigue and Fracture of Engineering Material and Structures*, 31:137–151.

Ewing, J. A. and Humfrey, J. C. (1903). The fracture of metals under repeated alternations of stress. *Phil. Trans. Royal Society*, CC:241–250.

Fedelich, B. (1998). A stochastic theory for the problem of multiple surface crack coalescence. *International Journal of Fracture*, 91:2345.

Forsyth, P. (1961). A two stage process of fatigue crack growth. *Proc. Symp. Crack Propagation*, pages 76–94.

Hamam, R., Hild, F., and Roux, S. (2007). Stress intensity factor gauging by digital image correlation: Application in cyclic fatigue. *Strain*, 43:181–192.

Hoshide, T. and Socie, D. (1988). Crack nucleation and growth modeling in biaxial fatigue. *Engineering Fracture Mechanics*, 29:287–.

Hua, C. and Socie, D. (1984). fatigue damage in 1045 steel under constant amplitude biaxial loading. *Fatigue Engng. Mater.Structure*, 7:165–179.

Le Pecheur, A. (2008). *Compréhension des mécanismes et prévision de l'amorçage en fatigue thermique des aciers austénitiques, prenant en compte l'état de surface et le caractère multi-axial du chargement.* PhD thesis, Ecole Centrale de Paris.

Li, Y. (for 2011). *Contribution à l'étude de l'endommagement par fatigue à l'aide d'un modèle polycristallin.* PhD thesis, Ecole Centrale de Paris.

Lindborg, U. (1969). A statistical model for the linking of microcracks. *Acta Matalurgica*, 17:521–526.

Ma, B. and Laird, C. (1989). Overview of fatigue behavior in copper single crystals (parts 1 to 5). *Acta Metallurgica*, 37(2):325–379.

Magnin, T., Coudreuse, L., and Lardon, J. (1985). A quantitative approach to fatigue damage evolution in fcc and bcc stainless-steels. *Scripta Metallurgica*, 19:1487–1490.

Maillot, V. (2003). *amorçage et propagation de reseaux de fissures de fatigue thermique dans un acier inoxydable austénitique de type X2 CrNi 18-09 (AISI 304L)*. PhD thesis, Ecole Centrale de Lille.

Malésys, N. (2007). *Modélisation probabiliste de la formation de réseaux de fissures en fatigue thermique*. PhD thesis, Ecole Normale Suprieure de Cachan.

Malésys, N., Vincent, L., and Hild, F. (2009). A probabilistic model to predict the formation and propagation of crack networks in thermal fatigue. *International Journal of Fatigue*, 31:565–574.

Man, J., Obrtlik, K., Blochwitz, C., and Polak, J. (2002). Atomic force microscopy of surface relief in individual grains of fatigued 316l austenitic stainless steel. *Acta Materialia*, 50:3767–3780.

Miller, K. (1997). the thresholds for crack propagation. *Fatigue and Fracture ASTM STP 1296*, 27:267–286.

Mughrabi, H., Ackermann, F., and Kerz, H. (1979). Persistent slip bands in fatigued face-centered and body-centered cubic metals. *Fatigue Mechanisms, ASTM STP*, 675:69–105.

Mughrabi, H., Wang, R., Differt, K., and Essman, U. (1983). Fatigue crack initiation by cyclic slip irreversibilities in high-cycle fatigue. *Fatigue mecha-*

nisms : Advances in quantitative measurement of physical damage, ASTM STP, 811:5–45.

Mura, T. (1994). A theory of fatigue crack initiation. *Materials Science and Engineering*, A176:61–70.

Osterstock, S. (2008). *Vers la prediction de l'apparition de reseaux de fissures en fatigue thermique : influence des parametres microstructuraux sur la dispersion à l'amorçage*. PhD thesis, Ecole Centrale de Lille.

Osterstock, S., Robertson, C., Sauzay, M., Degallaix, S., and Aubin, V. (2007). Prediction of the scatter of crack initiation under high cycle fatigue. *Mechanical Behavior of Materials X, Pts 1and 2*, 345-346:363–366.

Paris, P. and Erdogan, F. (1963). A critical analysis of crack propagation laws. *Journal of Basic Engineering, Transaction of the ASME*, pages 528–534.

Polak, J. and Zezulka, P. (2005). Short crack growth and fatigue life in austenitic-ferritic duplex stainless steel. *Fatigue and Fracture of Engineering Materials and Structures*, 20:923–935.

Poncelet, M., Barbier, G., Raka, B., Courtin, S., Desmorat, R., Le-Roux, J., and Vincent, L. (2010). Biaxial high cycle fatigue of a type 304l stainless steel: Cyclic strains and crack initiation detection by digital image correlation. *European Journal of Mechanics A/Solids*, 29:810–825.

Sauzay, M., Evrard, P., Steckmeyer, A., and Ferrié, E. (2010). Physically-

based modeling of the cyclic macroscopic behaviour of metals. *Procedia Engineering, fatigue 2010*, 2:531–540.

Suh, C., Lee, J., Kang, Y., Ahn, H., and Woo, B. (1992). A simulation of the fatigue crack process in type-304 stailess steel at 538-degrees-c. *Fatigue and Fracture of Engineering Materials and Structures*, 15:671–684.

Sutton, M. A., Helm, J. D., and Boone, M. L. (2001). Experimental study of crack growth in thin sheet 2024-t3. *International Journal of Fracture*, 109:285–301.

Vasek, A. and Polak, J. (1991). Low-cycle fatigue damage accumulation in armco-iron. *Fatigue and Fracture of Engineering Materials and Structures*, 14:193–204.

Weiss, J. (1992). *Endommagement en viscoplasticité cyclique sous chargement multiaxial à haute température d'un acier inoxydable austénitique*. PhD thesis, Ecole des Mines de Paris.

Weiss, J. and Pineau, A. (1993). Fatigue and creep-fatigue damage of austenitic stainless-steels under multiaxial loading. *Metallurgical Transactions a-Physical Metallurgy and Materials Science*, 24:2247–2261.

Zhai, T., Wilkinson., A. J., and Martin, J. W. (2000). A crystallographic mechanism for fatigue crack propagation through grain boundaries. *Acta materialia*, 48:4917 4927.